Analyst

Accepted Manuscript

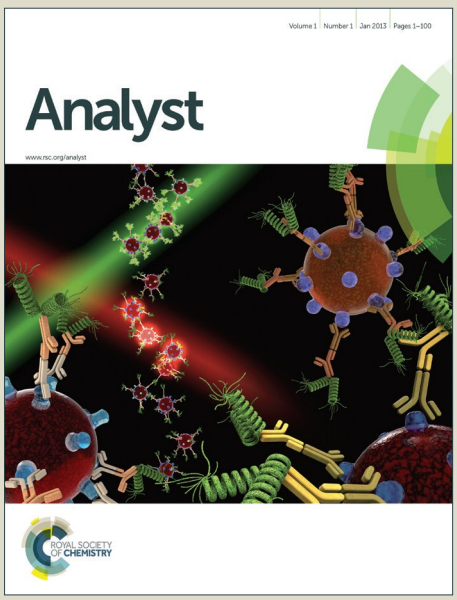

ROYAL SOCIETY OF CHEMISTRY

www.rsc.org/analyst

Factors influencing polyelectrolyte-aptamer multilayered films with target-controlled permeability for sensing applications

*Brian Malile and Jennifer I. L. Chen**

Department of Chemistry, York University, 4700 Keele Street, Toronto, ON, Canada M3J 1P3

*E-mail: jilchen@yorku.ca

KEYWORDS. Plasmonic sensor, polyelectrolyte multilayer, aptamer, permeability, structural change, electrochemical detection, aptasensor, interferences

ABSTRACT

Portable, easy-to-use and cost-effective sensing devices are desirable in healthcare, environmental monitoring and food safety. Herein we employ polyelectrolyte-aptamer (PE-aptamer) multilayered films that exhibit target-responsive permeability for colorimetric and electrochemical sensing. We present the quantitative detection of an exemplary small molecule, quinine, and address the potential for detection in complex media by examining interference effects. We optimize the film composition and investigate the importance of the structural-switching ability of the aptamer. The results from both platforms are corroborated to provide an outlook on the applicability of the PE-aptamer film for sensing. The label-free detection combined with the readily adaptive assembly process could be invaluable for diverse analytical fields.

INTRODUCTION

Detection tools that provide rapid results are desirable in healthcare, environmental analysis, food safety and homeland security.[1] The development of portable, low cost, and versatile sensors allows for field analysis[2] and point-of-care diagnosis.[1, 3] Numerous colorimetric sensors employ localized surface plasmon resonance (LSPR)[4,5] of nanoparticles and their conjugation with chemically modified biological probes. A colorimetric response is generated upon aggregation of nanoparticles[6-8] or changes in the morphology of the nanoparticles via their direct interaction with the analyte.[9] These solution-based nanoparticle sensors may pose limitations on portability and storage. Similarly, electrochemical sensors employ tagged biomolecular probes and may require the analytes to be redox-active to produce a signal. These approaches limit the types of analytes that can be detected, in addition to the complex surface chemistry for producing the active sensing layer with consistency. Hence, there is a need to develop novel methods of fabricating target-responsive thin films that can be readily adapted to a variety of substrates used in a range of sensing platforms.

Recent work exploits target-responsive polyelectrolyte-aptamer (PE-aptamer) multilayered films for sensing and cargo delivery applications.[10-12] Conventional polyelectrolyte films consist of polymers with oppositely charged groups, such as polyallylamine hydrochloride (PAH) and polystyrene sulfonate (PSS). They are deposited via layer-by-layer assembly on flat substrates or spherical templates.[13] These films are dynamic and responsive to physicochemical stimuli. They can respond to changes in the ionic strength and pH, and can distinguish between different types of ions.[14,15] An advantage of these films is that charged species can be easily incorporated to introduce new features thus allowing for a wide range of applications.[16] For example, DNA with its phosphate backbone can be incorporated into the multilayers.[17] A class

of oligonucleotides known as aptamers can bind to specific targets with high affinity.[18] They are obtained through Systematic Evolution of Ligands by Exponential Enrichment (SELEX) and may undergo structural switching upon binding. When aptamers are incorporated into polyelectrolyte films, the binding of target has been shown to regulate the diffusion and permeability of molecules. In this work, we elucidate the factors governing the functionality to provide the blueprint for their use in sensing applications.

Previously we presented a colorimetric sensor based on the morphological changes of the plasmonic nanoparticles controlled by the PE-aptamer film.[12] The PE-aptamer film swells more when the target is bound, leading to a higher diffusion rate of etchant molecules that alter the shape and size of the embedded nanoparticles. The high dependence of LSPR on the morphology of silver nanoprisms[19] leads to the generation of a colorimetric signal. Importantly, the analyte need not interact with the nanoparticles and the platform is entirely label-free. Herein we examine the quantitative and qualitative responses of two types of sensors incorporating the PE-aptamer film by employing optical spectroscopy and cyclic voltammetry. We investigate the interference effects from other ions, and the structural requirement of the aptamer to achieve the sensing functionality. By optimizing the film composition, we show that detection of the target can be achieved using different sensing platforms. The flexibility to incorporate different aptamers combined with facile fabrication make it a valuable cost-effective methodology for diverse sensing applications.

RESULTS AND DISCUSSION

Principle of detection

Scheme 1 illustrates our methodology. The PE-aptamer film comprising $(PAH/PSS)_4(PAH/DNA\text{-}aptamer)_8(PAH)$ (where the subscript indicates the number of bilayers) was deposited onto the substrate via layer-by-layer assembly. We chose PAH because it allows

effective buildup of the multilayers with DNA aptamer as compared to other strong polyelectrolyte (Fig. S1). The salt concentration (0.2 M NaCl) employed results in the deposition of polyelectrolytes in random coil conformation[20] with thicknesses of 3.8 nm and 1.8 nm per PAH/PSS and PAH/DNA bilayer, respectively.[12] The substrate either consists of gold-coated silver nanoprisms immobilized on a glass coverslip for the colorimetric sensor (scheme 1a), or ITO for the electrochemical sensor (scheme 1b). The MN19 aptamer binds to quinine or cocaine via the formation of a three-way junction.[21] We chose to work with this model aptamer to investigate the factors influencing the permeability of the PE-aptamer film because the non-absorbing target (quinine) allows us to characterize the concentration-dependent color changes in detail; the sensor may also have the potential for detecting narcotics. Upon exposure to the analyte solution, we use the ferricyanide ion as the chemical developer for both colorimetric and electrochemical sensors. Ferricyanide acts as an oxidizing agent that etches the nanoparticles[22] in the colorimetric platform, and serves as the redox-active probe for the electrochemical measurements. The results from the two platforms are corroborated to provide a universal outlook on the application of the target-responsive PE-aptamer film.

Colorimetric sensing via morphological changes of plasmonic nanoparticles

The colorimetric platform consists of a glass substrate with immobilized nanoparticles, on top of which the PE-aptamer film was deposited. The films were first incubated with the solution of interest, then rinsed and immersed in ferricyanide solution to obtain the colorimetric response. The charge of the ion is one of the factors influencing its diffusion through a polyelectrolyte multilayered film.[23,24] We hypothesized that the high charge of the ferricyanide complex may prove advantageous for enhancing the difference in the diffusion kinetics between the control (water) and target-bound (quinine) films. All films were capped with PAH to

facilitate the diffusion and partitioning of ferricyanide through the PE-aptamer film (Fig. S2). Fig. 1(a) and 1(b) show the evolution of the extinction spectra of the plasmonic sensor during etching by 60 μM of $K_3Fe(CN)_6$ over 35 min for films incubated in water and 500 μM of quinine, respectively. The LSPR peak decays and slightly redshifts from the initial peak of 620 nm as etching proceeds. The decrease in intensity results from the rounding and decreasing in size of the nanoparticles as seen in the TEM images (Fig. S3). Fig. 1(c) summarizes the intensity decay at 620 nm for the two films: a more rapid and greater decay is observed for film exposed to quinine compared to the control film. Notably the difference is already discernible within 2 minutes of chemical development: the film with quinine-bound shows a decay of ~35% while the intensity of the control film only drops by ~17%. We consequently use the initial intensity decay as a measure of the optical response and examine different concentrations of quinine, as shown in Fig. 1(d). We observe a higher percent of intensity decay with increasing quinine concentration, with a saturation response of ~30% for > 250 μM quinine. The colorimetric response can be discerned by eye, as shown in the photographs in the inset of Fig. 1(d). After etching, the films exposed to lower quinine concentrations (0 μM and 100 μM) appear blue, while films exposed to 250 μM and 500 μM quinine have a grayish blue colour with lower intensity.

These results show that the binding of quinine to the PE-aptamer film leads to a faster etching rate of nanoparticles due to an increase in the diffusion of the ferricyanide ions. The use of ferricyanide as the chemical etchant is effective and yields similar results as our previous study in which we used iodide/triiodide as the etchant. However, in the current work the colour change is not as significant and consists mainly as a decrease in intensity. This difference may arise due to different surface chemistry that dampens plasmons and influences the colour change.

In solution, the etching of bare nanoparticles with ferricyanide causes a blue-shift in the LSPR peak position[25] (see Fig. S4), though this change is not observed for nanoparticles covered with PE-aptamer films. One possibility is that the reaction products remain on the surface of the nanoparticles leading to a decrease in intensity and a red-shift in the LSPR peak. Variations in the nanoparticle morphology and the surface coverage with PE-aptamer can also give rise to variations in the colorimetric response.

As $Fe(CN)_6^{3-}$ is redox active, we then adapted the PE-aptamer multilayered film into an electrochemical sensor and characterize the response using cyclic voltammetry. The electrochemical response can then corroborate the enhanced diffusion rate of ions and the response of the colorimetric sensor.

Electrochemical sensing using cyclic voltammetry

Cyclic voltammetry (CV) provides information on the diffusion of a redox active species to the electrode. Under quiescent condition, the diffusion coefficient of a molecule is related to the peak current[26] by:

$$i = 2.686 \times 10^5 \, n^{\frac{3}{2}} A c D^{1/2} v^{1/2}$$

where i is the peak current; n is the number of electrons; A is the electrode area; D is the diffusion coefficient; ν is the scan rate and C is the concentration. Electrochemical studies have been performed for the study of conventional polyelectrolyte multilayers[14, 27], though not extensively for those comprising aptamers. We assembled the films on patterned ITO electrodes, and measured the voltammograms of films as-deposited and after incubation with the solution of interest, i.e. water as control and quinine as the analyte solution. The measurement of the as-deposited films provides information on the integrity of the PE-aptamer film – a uniformly

deposited film typically has peak currents of 0.2 - 0.5 μA, while that of poorly formed films, likely with pin holes, showed much higher currents and were discarded. Fig. 2(a) and 2(b) show the cyclic voltammograms for as-deposited electrodes and after incubation with water and quinine, respectively. The increase in peak current after incubation in water can be attributed to the swelling of the film upon hydration where some restructuring of the interpenetrated layers could arise due to the mobility of the low molecular weight materials or smoothing effect.[14, 24] On the other hand the change in the peak current measured after incubation with quinine is much greater than that with water. We calculate the difference in anodic peak currents ($\Delta I_{p,a}$) before and after incubation as the electrochemical response. The binding of quinine leads to a twofold increase in the $\Delta I_{p,a}$ compared to the control (0.42 ± 0.05 μA vs 0.19 ± 0.02 μA). To a first-approximation, this increase in the peak current suggests a 4.9 fold increase of the diffusion rate when quinine is bound to the aptamer film. The similar twofold increase in response between the colorimetric and voltammetric sensors corroborate the change in the permeability of the PE-aptamer film and the enhanced diffusion of ferricyanide as the origin of detection. We then carried out concentration-dependence study as shown in Fig. 2(c). The $\Delta I_{p,a}$ increases with increasing concentration of quinine. Fitting with a single-site binding model[28] yields a K_D of 56.2 ± 18.2 μM. This K_D is about two orders of magnitude higher than that of the free aptamer in solution, which could be due to the immobilization of the aptamer in the film.[17] In comparison to the colorimetric platform, the electrochemical platform shows better reproducibility and quantitative analysis because of the less complex surface reactions. Improvements on the uniformity and surface roughness of ITO substrates would further be beneficial.

Next we probed the specificity of the sensing platform using a cocaine metabolite Ecgonine. Ecgonine has a bicyclic ring present in quinine and cocaine, however it does not bind

to the aptamer.[29,30] The $\Delta I_{p,a}$ for Ecgonine is 0.22 ± 0.05 μA, close to that of water 0.19 ± 0.03 μA (Fig. 2d). The aptamer retains its specificity when incorporated into thin films. Additional control experiments using a random sequence of DNA instead of the aptamer show negligible change in the response after incubation with quinine (Fig. S5). These results confirm that the interaction of quinine with the MN19 aptamer gives rise to the sensing capability and that the activity of the aptamer is retained

Optimization of the polyelectrolyte film composition

We examined different compositions of the film by varying the number of base bilayers (PAH/PSS) and target binding bilayers (PAH/DNA-aptamer) to optimize the electrochemical response. Fig. 3(a) shows the anodic peak current ($I_{p,a}$) for the electrodes covered with increasing number of PAH/PSS bilayers without changing the number of PAH/DNA-aptamer bilayers. The multilayers of PAH-DNA-aptamer alone are too permeable to achieve any target-controlled diffusion, and hence base layers of PAH/PSS are needed. With less than two bilayers of PAH/PSS, there is negligible difference between electrodes with or without exposure to quinine. This observation is in line with previous reports that the first couple bilayers of PAH/PSS are thinner and more permeable and deposit differently than subsequent layers.[27, 31-33] Once four bilayers of PAH/PSS are deposited, the $I_{p,a}$ between electrodes incubated in water vs quinine differ significantly, showing the sensitivity of the film to quinine. These results show that at least four base bilayers of PAH/PSS are necessary to achieve a significant response. We also varied the number of target-binding bilayers (PAH/DNA-aptamer) from 4, 8 to 12 on top of four bilayers of PAH/PSS. Fig. 3(b) shows a slight increase in the electrochemical response with increasing number of layers of the aptamer, although there appears only a limited effect on the permeability of the film by increasing the number of bilayers DNA aptamer beyond four.

Interferences

The ability of a sensor to work in complex media makes it highly desirable for field analysis such as environmental monitoring where minimal sample preparation is desired. Polyelectrolyte multilayered films shave been studied as nanofiltration membranes due to their interaction with various ions.[24,34] These films are also responsive to changes in ionic strengths and the presence of ions[35] as the layers are held together by electrostatic forces. Heavy metal ions such as lead (II), tin (II), and mercury (II) have also been known to interact with DNA.[36-38] Hence, we carried out ion interference experiments to investigate the practicality of the PE-aptamer films for sensing. The films for both platforms were incubated with various ions and then rinsed and measured. Fig. 4(a) and 4(b) show the response from the colorimetric and electrochemical sensing platforms, respectively. Fig. 4(a) shows that most ions do not affect the colorimetric response – producing an intensity decay close to 15%, which is comparable to the control (water). On the other hand, sulfate is a significant interference, giving rise to a false positive response with a plasmonic intensity decay of ~33%, which is similar to quinine. Additionally no colorimetric response was achieved when the film was exposed to Hg^{2+}. The absence of nanoparticle etching upon Hg^{2+} exposure could arise due to the amalgamation and reaction with silver.[39,40] Fig. 4(b) summarizes the ionic interference effects on the electrochemical platform, which has similar trends as Fig. 4(a). Most ions and heavy metals do not interfere and yield $\Delta I_{p,a}$ close to that of control. Notably the response of sulfate is again high, with a $\Delta I_{p,a}$ of 0.55 ± 0.05 μA. Control experiments show that the interaction of sulfate is with the polyelectrolytes rather than the DNA-aptamer (Fig. S6). It is plausible that sulfate ion affects the crosslinking of the polyelectrolyte layers by binding to the amine groups of PAH. We were able to decrease the amount of interference of sulfate by precipitating it with $BaCl_2$ prior to

detection (see Fig. S7) - the false positive response can be reduced by pre-treatment of the analyte solution if needed. Importantly as the sensing mechanism involves two stages, in which the exposure to analyte solution is separated from signal generation, effects of environmental factors such as temperature, ionic strength and pH, would be minimal unless they cause irreversible changes to the film. The stability of the PE-aptamer multilayered films in ionic solutions suggest potential applications such as monitoring contaminants in lake waters and detecting metabolites in bodily fluids such as urine.

Effect of aptamer folding

It has been suggested that the increase in permeability of the film upon target binding arises from a structural change of the aptamer.[17,41, 42] We investigate this factor by using different aptamers for quinine. Various aptamer sequences for quinine/cocaine have been identified with pre-folded or random structure in the absence of the target. For example, MN4 – an aptamer with 6 additional nucleotides compared to MN19 – does not undergo structural change and folds into a threeway junction even without the target. Fig. 5(a) shows the structures of MN19 and MN4 aptamers before and after binding; they bind to quinine with similar K_D (0.7 ± 0.2 μM and 0.23 ± 0.03 μM for MN19 and MN4 in solution respectively).[43] The different nature of the aptamers therefore allows us to probe the importance of the structural change for inducing the change in the permeability of the target-responsive film. Fig. 5(b) shows the $\Delta I_{p,a}$ of films comprising of either aptamer after incubation in water and quinine. The films with MN19 show significantly different $\Delta I_{p,a}$ with or without quinine-bound (0.19 ± 0.02 μA vs 0.42 ± 0.5μA). In contrast, the films with MN4 do not show a significant difference with or without quinine (0.37 ± 0.08 μA vs 0.40 ± 0.05 μA). This observation suggests that conformational change of the aptamer is important. It is likely that the folding of the aptamer leads to a rearrangement of the charges in

the film and consequently influences the mass transport and hopping of the ferricyanide ions through the film.[44]

EXPERIMENTAL

Materials

Silver nitrate ($AgNO_3$), sodium borohydride ($NaBH_4$), sodium citrate dihydrate, L-ascorbic acid, hydrogen peroxide 30 wt%, polyvinylpyrrolidone (PVP) MW 96000, diethylamine, potassium iodide, hydrogen tetrachloroaurate (III) trihydrate ($HAuCl_4 \cdot 3H_2O$), aminopropyltrimethoxysilane (APTMS), polyallylamine hydrochloride (PAH) MW 56000, polystyrenesulphonate (PSS) MW 100000, and quinine HCl were purchased from Sigma Aldrich. Indium Tin Oxide (ITO) coated glass was obtained from Delta Technologies. DNA sequences of MN-19 (*5' - GAC AAG GAA AAT CCT TCA ACG AAG TGG GTC- 3 '*) , MN4 (*5'- GGC GAC AAG GAA AAT CCT TCA ACG AAG TGG GTC GCC-3'*) and random sequence (*5'- GAC ACG CAC ACT GTC GCC GAC T-3'*) were purchased from IDTDNA.

Aqueous solutions of $MgCl_2$, $MgSO_4$, $NaHPO_4$, NH_4Cl, LiCl, $PbCl_2$, $HgCl_2$, $SnCl_2$, $NaSO_4$ and KCl at 500 μM or 1 mM were used in the ionic interference experiment.

Synthesis of gold-coated silver nanoprisms

In a typical synthesis of silver nanoprisms (AgNP)[45], 50 mL of 0.1 mM silver nitrate was mixed with 3 mL of 30 mM of sodium citrate dihydrate under vigorous stirring. A volume of 120 μL of H_2O_2 30 wt% was then added. Immediately after the addition of H_2O_2, fresh 200 or 180 μL of 0.1 M $NaBH_4$ was added. The reaction was then allowed to proceed for 30 min. The colloidal solution was centrifuged and washed with 1 mL of 3 mM sodium citrate once. The nanoparticles were dispersed in 9 mL of H_2O. To proceed with the vertical growth, 1 mL PVP at 0.0175 M and 37.5 μL of 0.5 M ascorbic acid were added to the redispersed particles. Then, a volume of 0.6

mL of 0.6 mM of $AgNO_3$ was added via a syringe pump at 6 mL/h. The AgNP were then grown laterally to acquire the desired LSPR wavelength (540 – 560 nm) by adding a solution 300 µL of 30 mM citrate and a growth solution of 0.75 mM $AgNO_3$ and 1.13 mM citrate via a syringe pump at 6 mL/h. UV-Vis spectra were taken to monitor the size of the nanoparticles. The reaction was allowed to proceed for 1 hour.

Gold-coating was achieved using previously reported method.[46] A volume of 1 mL of PVP at 5 wt%, 200 µl of 0.5 M ascorbic acid, and 150 µL of diethylamine were added to the AgNP solution. A separate gold solution consisting of 1.37 mL of H_2O, 100 µL 5% PVP, 20 µL of 0.2 M KI, and 5µL of 0.25 M of $HAuCl_4 \cdot 3H_2O$ was added through a syringe pump at a rate of 1 mL/h. Upon completion, the reaction was allowed to proceed for 0.5 -1 h. The gold-coated AgNP were cleaned via centrifugation and were redispersed in 1 mL of H_2O for storage.

Preparation of APTMS-functionalized cover slips and deposition of AgNP on glass

The cover slips (VWR micro cover glass 25 mm x 25 mm) were placed in the plasma cleaner (Harrick's PDC-32G) for 15-20 minutes and then immersed in 50 mL of a 1% ethanolic solution of APTMS for 2 h. The cover slips were then rinsed, dried and placed on a hot plate for annealing under nitrogen atmosphere overnight. The coverslip was cut to six pieces for the fabrication of the colorimetric sensor. Gold-coated AgNP were deposited by repeated immersion of the substrate into the colloidal solution followed by rinsing and drying after each step.

Layer-by-layer assembly of polyelectrolyte on AgNP films

Solutions of PAH and PSS were made by dissolving 2 mg/mL of polyelectrolyte in 0.2 M NaCl. DNA aptamer was dissolved in a 1x Phosphate Buffer Saline (PBS) solution with 0.2 M NaCl at a concentration of 4.5 µM. Layer-by-layer assembly was carried out using a robotic

dipper (Microm DS 50). In a single layer deposition, the films were placed for 10 minutes in the polyelectrolyte solution followed by two rinsing steps. Depending on the architecture of the film, different polyelectrolyte solutions were used. The films were finally capped with a single layer of PAH. The films were kept hydrated at all times.

Colorimetric detection

The PE-aptamer covered plasmonic films were immersed in the solution of interest for 1 h. The films were then rinsed and developed using 60 μM of $K_3(Fe(CN)_6$. UV-vis spectra were taken every five minutes for 35 minutes using a Cary 100 Bio spectrophotometer. Typically, the results from at least six films were acquired for each condition and their averages and standard error of the mean were calculated.

Electrochemical detection

The ITO substrates were patterned using a Versa Laser. The size of the electrodes was 3 mm in diameter. The electrodes were rinsed and sonicated for 10 minutes in acetone to remove any organic residues from the surface. After sonication, they were placed in RCA bath for 10 minutes at 80 °C for further cleaning and activation of the surface. The assembly of the polyelectrolyte aptamer film was the same as that of the colorimetric study.

An ER466 integrated potentiostat system (eDAQ) was used for cyclic voltammetry experiments. A three-electrode system in a cell containing ~7 mL of electrolyte solution (60 μM ferricyanide, 6 mM KCl), a Pt wire counter electrode and Ag/AgCl reference electrode was used. The solution was degassed and the film was equilibrated in the redox electrolyte solution for 5 min prior to the CV scan. The potential was scanned from -0.35 V to 0.7 V at 0.1 V s^{-1}. An initial cyclic voltammetry scan was performed on all as-deposited electrodes. The electrodes were then

incubated with the solution of interest for 30 min, followed by rinsing and cyclic voltammetry again. The difference in the anodic peak current was calculated as the electrochemical response ($\Delta I_{p,a}$).

CONCLUSIONS

We have demonstrated the versatility of adapting the PE-aptamer multilayered film for both colorimetric and electrochemical sensing platforms. Binding of the target alters the aptamer structure and thereby the permeability of the film. Changes in the diffusion rate of ferricyanide, which was employed as the chemical developer for both platforms, leads to different etching kinetics of the plasmonic nanoparticles and voltammetric peak currents, thereby generating the colorimetric and electrochemical responses. These two sensing platforms show similar detection range and the capability to perform in a wide range of ions, including ammonium, halides, alkali, alkaline and heavy metals. Importantly, we show that the aptamer must undergo structural changes to achieve the permeability-gating functionality. With the large library of aptamers developed and the ease of layer-by-layer assembly on different substrates, we believe these PE-aptamer films have the potential to be a universal component for various sensing devices and the versatility to be tailored to a wide range of analytes. Furthermore, the fundamental understanding of these thin films should provide insight on their use in other areas including nanofiltration membranes and microcapsules.

ACKGNOWLEDGMENTS

This work is supported by Natural Science and Engineering Research Council of Canada (NSERC Discovery Grant), Canada Foundation of Innovation (JELF grant) and Province of Ontario (ORF grant). The authors thank S. Zhu and K. Rethoret for technical assistance and P. Johnson for discussions.

Supporting Information. Electronic Supplementary Information (ESI) available. See

DOI: 10.1039/b000000x

REFERENCES

1. D. A. Giljohann and C. A. Mirkin, *Nature*, 2009, **462**, 461-464.
2. M. E. Germain and M. J. Knapp, *Chem. Soc. Rev.*, 2009, **38**, 2543-2555.
3. J. Wang, *Biosens. Bioelectron.*, 2006, **21**, 1887-1892.
4. N. Nath and A. Chilkoti, *Anal. Chem.*, 2002, **74**, 504-509.
5. J. Liu and Y. Lu, *Nat. Protocol.*, 2006, **1**, 246-252.
6. D. Vilela, M. C. González and A. Escarpa, *Anal. Chim. Acta.*, 2012, **751**, 24-43.
7. N. T. K. Thanh and Z. Rosenzweig, *Anal. Chem.*, 2002, **74**, 1624-1628.
8. J. Liu and Y. Lu, *Angew. Chem. Int. Ed.*, 2006, **45**, 90-94.
9. X. Wang, L. Chen and L. Chen, *Microchim. Acta*, 2014, **181**, 105-110.
10. Y. Du, C. Chen, B. Li, M. Zhou, E. Wang and S. Dong, *Biosens. Bioelectron.*, 2010, **25**, 1902-1907.
11. W.-C. Liao, C.-H. Lu, R. Hartmann, F. Wang, Y. S. Sohn, W. J. Parak and I. Willner, *ACS Nano*, 2015, DOI: 10.1021/acsnano.5b03223.
12. B. Malile and J. I. L. Chen, *J. Am. Chem. Soc.*, 2013, **135**, 16042-16045.
13. G. Decher and J.-D. Hong, *Makromol. Symp.*, 1991, **46**, 321-327.
14. M. Schönhoff, V. Ball, A. R. Bausch, C. Dejugnat, N. Delorme, K. Glinel, R. v. Klitzing and R. Steitz, *Colloid Surface A*, 2007, **303**, 14-29.
15. J. J. Harris, J. L. Stair and M. L. Bruening, *Chem. Mater.*, 2000, **12**, 1941-1946.
16. T. Boudou, T. Crouzier, K. Ren, G. Blin and C. Picart, *Adv. Mater.*, 2010, **22**, 441-467.
17. Y. Sultan, R. Walsh, C. Monreal and M. C. DeRosa, *Biomacromolecules*, 2009, **10**, 1149-1154.
18. S. E. Osborne and A. D. Ellington, *Chem. Rev.*, 1997, **97**, 349-370.

.

19. J. E. Millstone, S. J. Hurst, G. S. Metraux, J. I. Cutler and C. A. Mirkin, *Small*, 2009, **5**, 646-664.

20. D. Carrière, R. Krastev and M. Schönhoff, *Langmuir*, 2004, **20**, 11465-11472.

21. M. A. D. Neves, O. Reinstein, M. Saad and P. E. Johnson, *Biophys. Chem.*, 2010, **153**, 9-16.

22. Y. Xia, X.-M. Zhao, E. Kim and G. M. Whitesides, *Chem. Mater.*, 1995, **7**, 2332-2337.

23. L. Krasemann and B. Tieke, *Langmuir*, 2000, **16**, 287-290.

24. T. R. Farhat and J. B. Schlenoff, *Langmuir*, 2001, **17**, 1184-1192.

25. J. Zhai, Y. Zhai and S. Dong, *Colloid Surface A*, 2009, **335**, 207-210.

26. A. J. Bard and L. R. Faulkner, *Electrochemical methods: fundamentals and applications*, Wiley New York, 1980.

27. J. J. Harris and M. L. Bruening, *Langmuir*, 1999, **16**, 2006-2013.

28. M. McKeague, A. De Girolamo, S. Valenzano, M. Pascale, A. Ruscito, R. Velu, N. R. Frost, K. Hill, M. Smith, E. M. McConnell and M. C. DeRosa, *Anal. Chem.*, 2015, DOI: 10.1021/acs.analchem.5b02102.

29. A. Vaz, S. S. Lefkowitz, A. Castro and D. L. Lefkowitz, *Life Sci.*, 1994, **55**, PL439-PL444.

30. S. Slavkovic, M. Altunisik, O. Reinstein and P. E. Johnson, *Biorg. Med. Chem.*, 2015, **23**, 2593-2597.

31. S. T. Dubas and J. B. Schlenoff, *Macromolecules*, 1999, **32**, 8153-8160.

32. S. V. P. Barreira, V. García-Morales, C. M. Pereira, J. A. Manzanares and F. Silva, *J. Phys. Chem. B*, 2004, **108**, 17973-17982.

33. F. Caruso, K. Niikura, D. N. Furlong and Y. Okahata, *Langmuir*, 1997, **13**, 3422-3426.

34. A. E. El Haitami, D. Martel, V. Ball, H. C. Nguyen, E. Gonthier, P. Labbé, J.-C. Voegel, P. Schaaf, B. Senger and F. Boulmedais, *Langmuir*, 2009, **25**, 2282-2289.

35. S. L. Clark, M. F. Montague and P. T. Hammond, *Macromolecules*, 1997, **30**, 7237-7244.

36. J. R. N. McLean, D. H. Blakey, G. R. Douglas and J. G. Kaplan, *Mutat. Res. Lett.*, 1983, **119**, 195-201.

37. G. Wang, Q. Zhao, X. Kang and X. Guan, *J. Phys. Chem. B*, 2013, **117**, 4763-4769.

38. A. Hartwig, *Environ. Health Perspect.*, 1994, **102**, 45-50.

39. J. T. T. Pang and I. M. Ritchie, *Electrochim. Acta*, 1982, **27**, 683-689.

40. K. V. Katok, R. L. D. Whitby, T. Fukuda, T. Maekawa, I. Bezverkhyy, S. V. Mikhalovsky and A. B. Cundy, *Angew. Chem. Int. Ed.*, 2012, **51**, 2632-2635.

41. Y. Sultan and M. C. DeRosa, *Small*, 2011, **7**, 1219-1226.

42. L. Chen, X. Zeng, A. R. Ferhan, Y. Chi, D.-H. Kim and G. Chen, *Chem. Commun.*, 2015, **51**, 1035-1038.

43. O. Reinstein, M. Yoo, C. Han, T. Palmo, S. A. Beckham, M. C. J. Wilce and P. E. Johnson, *Biochemistry*, 2013, **52**, 8652-8662.

44. S. Han, B. H. Lindholm-Sethson, S., *Electrochim. Acta*, 1999, **45**, 845-853.

45. C. B. Gao, Z. D. Lu, Y. Liu, Q. Zhang, M. F. Chi, Q. Cheng and Y. D. Yin, *Angew. Chem. Int. Ed.*, 2012, **51**, 5629-5633.

46. J. Zeng, X. H. Xia, M. Rycenga, P. Henneghan, Q. G. Li and Y. N. Xia, *Angew. Chem. Int. Ed.*, 2011, **50**, 244-249.

FIGURES

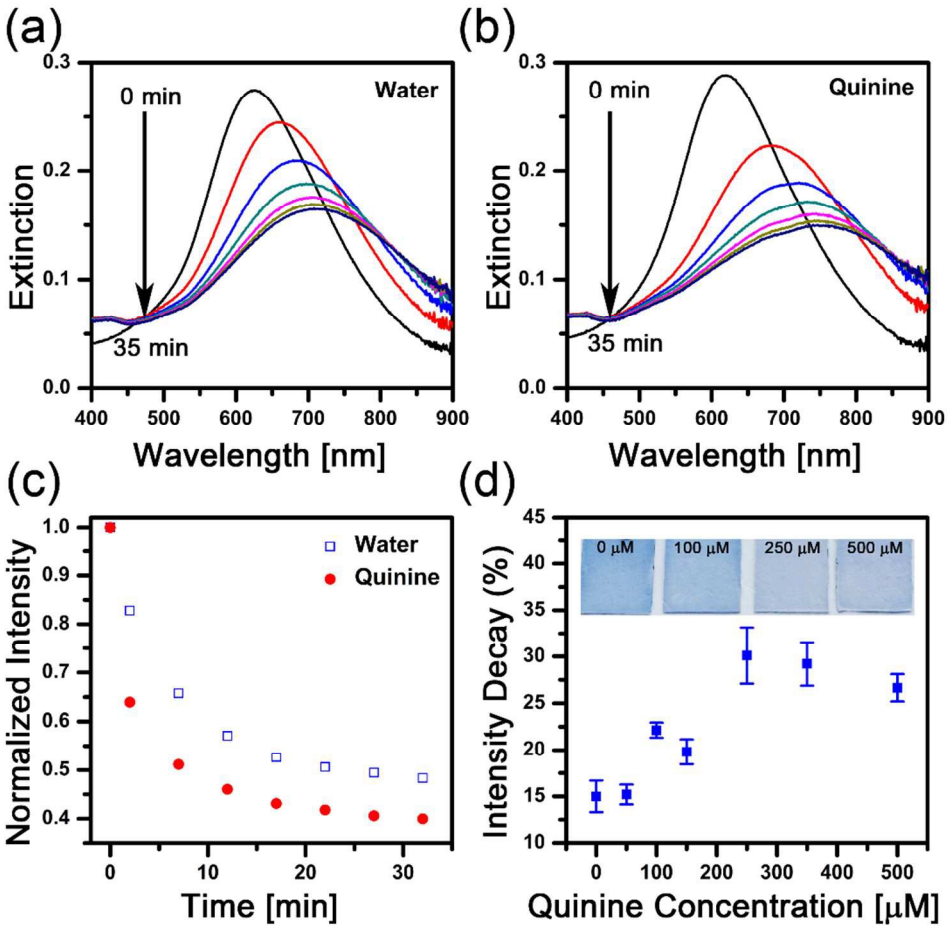

Fig. 1. Colorimetric response of Ag nanoprism films incorporated with PE-aptamer multilayers. Extinction spectra of the films exposed to water (a) and 350 μM quinine (b) during etching with 60 μM $K_3(Fe(CN)_6$. (c) Intensity decay of LSPR at 620 nm over time for the films. A faster decay in intensity is observed when the platform was incubated with quinine. (d) Initial intensity decay of films exposed to different concentrations of quinine for 1 hour. A total of 34 films were examined. Inset shows the photographs of the films.

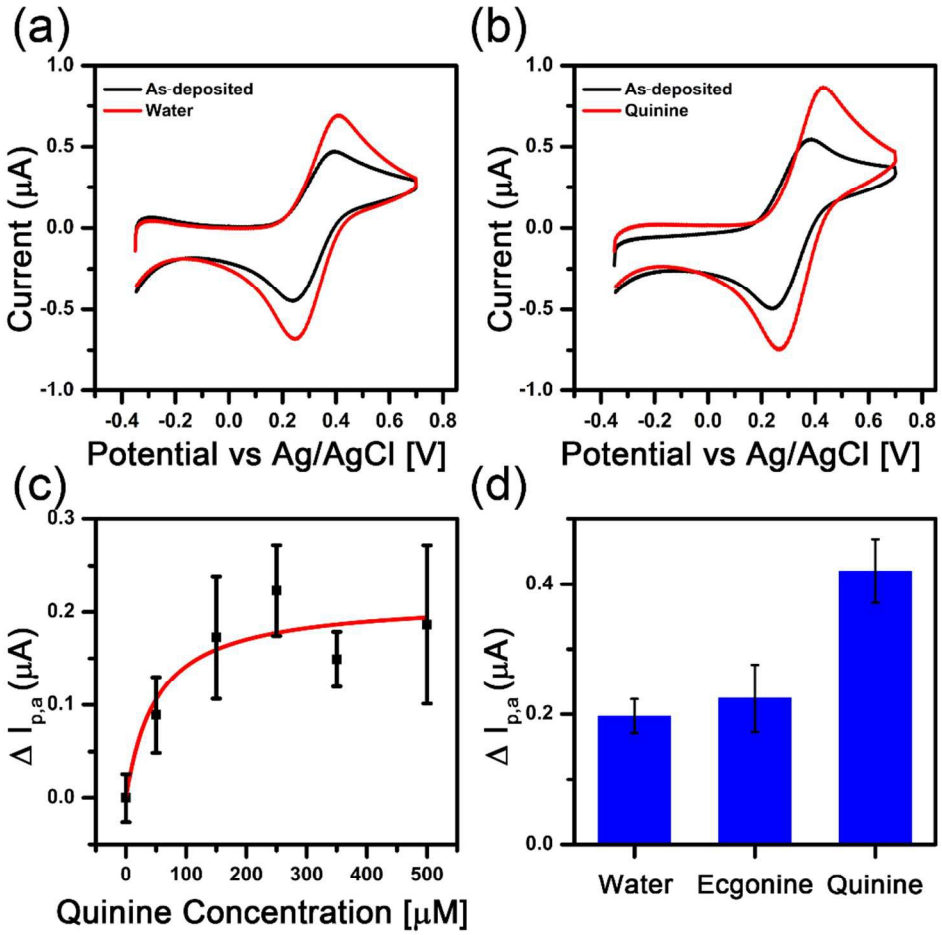

Fig. 2. Electrochemical characterization of the platform for the detection of quinine. Cyclic voltammograms of control H_2O (a) and 350 μM quinine (b): as-deposted PE-aptamer film (black) and after incubation with the solution (red). CV was performed in 60 μM $K_3(Fe(CN)_6$ with 6 mM KCl at a scan rate of 100 mVs^{-1}. A greater increase in peak current is observed for film with quinine bound. (d) Change in peak current ($\Delta I_{p,a}$) for different concentrations of quinine. An increase in quinine concentration leads to higher $\Delta I_{p,a}$. (e) A comparison of $\Delta I_{p,a}$ for control, quinine and ecgonine (350 μM) showing the specificity of the platform.

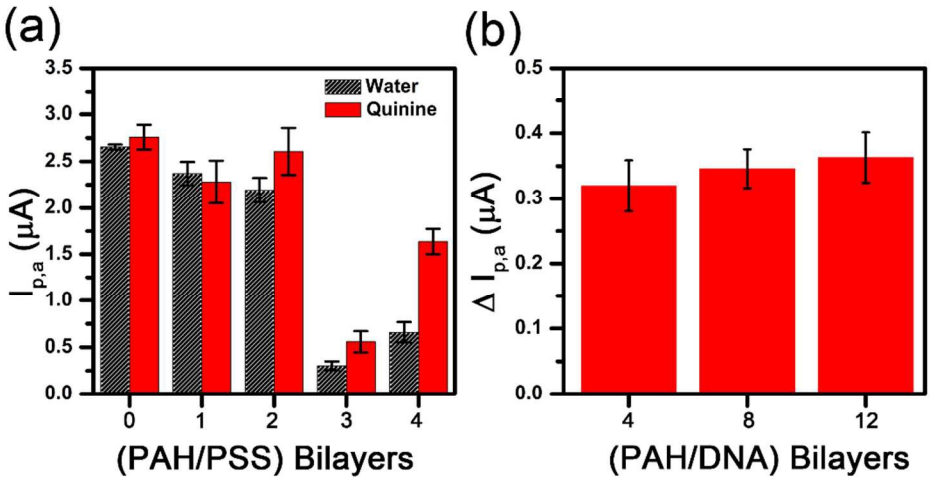

Fig. 3. Optimization of PE-aptamer multilayers. (a) Anodic peak currents after immersion in water and quinine for electrodes covered with increasing number of bilayers of PAH/PSS while keeping the top (PAH/DNA-aptamer)$_8$PAH constant. The largest difference between H_2O and quinine is observed for four bilayers of PAH/PSS. (b) Effect of increasing the number of PAH/DNA bilayers with four base bilayers of PAH/PSS on the $\Delta I_{p,a.}$

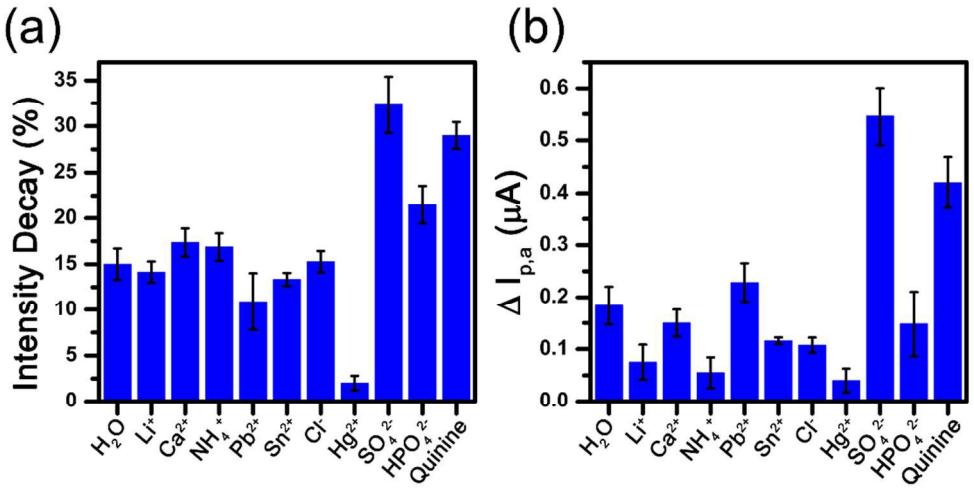

Fig. 4. Effects of ions on the sensing performance. (a) Colorimetric response, measured as percent of LSPR intensity decay, of various ions at 500 μM. (b) Electrochemical response, measured as $\Delta I_{p,a}$ for the ions at 1 mM. Sulfate is an interference and yields a false positive detection.

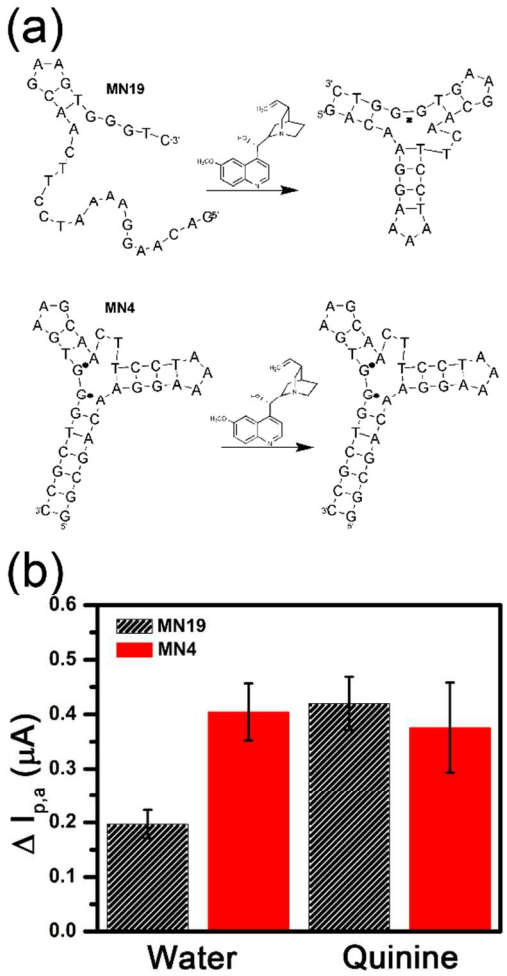

Fig. 5. Effect of structural-switching of the aptamer on the sensing capability. (a) Chemical structure of the cocaine/quinine-binding aptamers MN19 and MN4. MN19 with one pre-formed stem folds into a three-way junction upon binding to quinine. MN4 with an additional three base pairs prefolds into the three-way junction in the absence of quinine and does not undergo structural switching. (b) Electrochemical response ($\Delta I_{p,a}$) for the films comprising either MN19 or MN4 as the aptamer. No difference in $\Delta I_{p,a}$ between H_2O and quinine was observed when MN4 was employed, compared to a twofold increase in $\Delta I_{p,a}$ for that of MN19. A structural-switching aptamer is required for achieving a change in the permeability.

SCHEMES

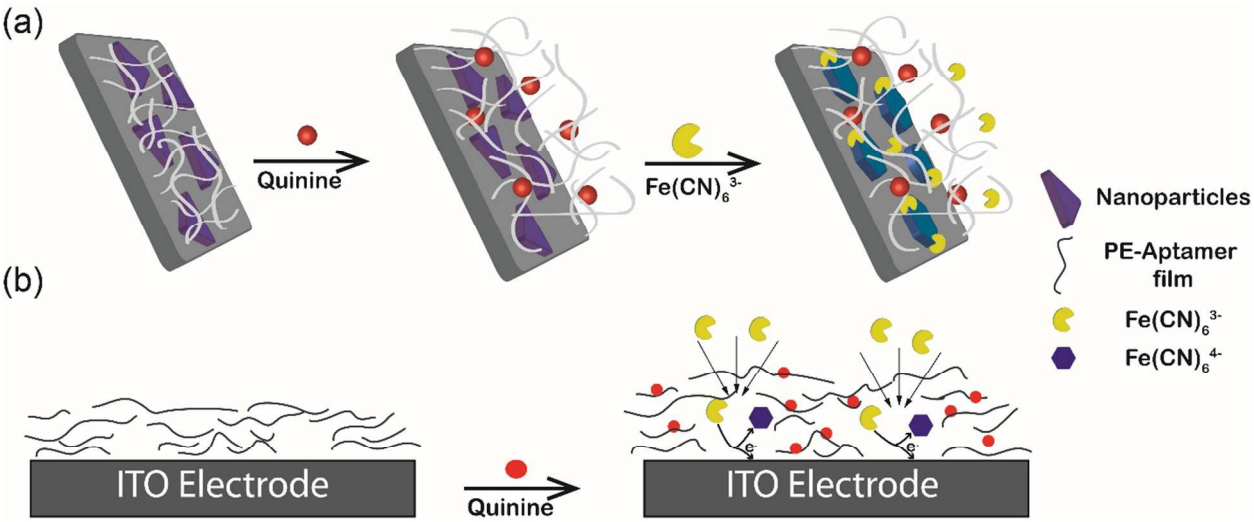

Scheme 1. Two sensing platforms employing the PE-aptamer multilayered film. (a) Colorimetric sensor comprising gold-coated silver nanoprisms on top of which the target-responsive PE-aptamer film is assembled. The aptamer binds to quinine and the film is subsequently developed by immersing with $Fe(CN)_6^{3-}$ as the nanoparticle etchant. (b) Electrochemical sensor fabricated by depositing PE-aptamer film on patterned ITO electrodes. Binding of quinine increases the diffusion of $Fe(CN)_6^{3-}$ to the electrode resulting in an increase in redox activity.

TABLE OF CONTENTS

We present target-controlled permeability change in polyelectrolyte-aptamer multilayered film as a universal basis for sensing. The enhanced diffusion of ions across the film upon target binding was employed to derive colorimetric or electrochemical response.

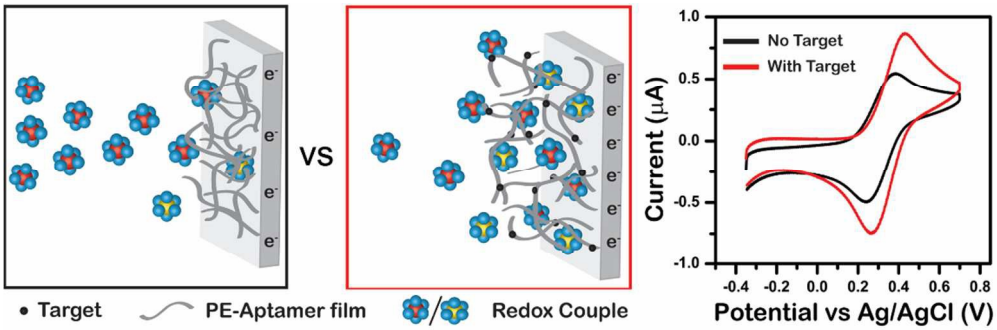

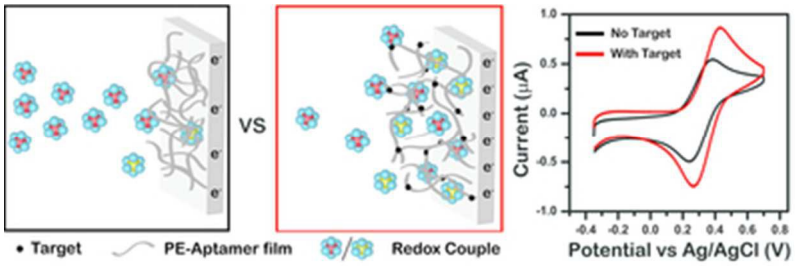

33x11mm (300 x 300 DPI)